Comparing canopy metrics derived from terrestrial and airborne laser scanning in a Douglas-fir dominated forest stand

Thomas Hilker [1*], Martin van Leeuwen[1], Nicholas C. Coops[1], Michael A. Wulder[4], Glenn J Newnham[2], David L.B. Jupp[3], Darius S. Culvenor[2]

[1]Faculty of Forest Resources Management, University of British Columbia, 2424 Main Mall, Vancouver, BC, V6T 1Z4, Canada.

[2]CSIRO Sustainable Ecosystems Private Bag 10, Clayton South, Victoria 3169, Australia

[3]CSIRO Marine and Atmospheric Research, GPO Box 3023, Canberra, ACT 2611, Australia

[4]Canadian Forest Service (Pacific Forestry Centre), Natural Resources Canada, 506 West Burnside Road, Victoria, BC, V8Z 1M5, Canada

* corresponding author:

Thomas Hilker

Phone: +1 (604) 827 4429, Fax :+1 (604) 822 9106, thomas.hilker@ubc.ca

Pre-print of published version.

Reference:

Hilker, T., van Leeuwen, M., Coops, N.C., Wulder, M.A., Newnham, G.J., Jupp, D.L.B., Culvenor, D.S. 2010. Comparing canopy metrics derived from terrestrial and airborne laser scanning in a Douglas-fir dominated forest stand. Trees-Structure and Function. 24: 819-832

DOI:

doi:10.1007/s00468-010-0452-7

Disclaimer:

The PDF document is a copy of the final version of this manuscript that was subsequently accepted by the journal for publication. The paper has been through peer review, but it has not been subject to any additional copy-editing or journal specific formatting (so will look different from the final version of record, which may be accessed following the DOI above depending on your access situation).

Abstract

Accurate estimates of vegetation structure are important for a large number of applications including ecological modeling and carbon budgets. Light detection and ranging (LiDAR) measures the three dimensional structure of vegetation using laser beams. Most LiDAR applications today rely on airborne platforms for data acquisitions, which typically record between 1 and 5 “discrete” returns for each outgoing laser pulse. While airborne LiDAR allows sampling of canopy characteristics at stand and landscape level scales, this method is largely insensitive to below canopy biomass such as understorey and trunk volumes as these elements are often occluded by the upper parts of the crown, especially in denser canopies. As a supplement to airborne laser scanning (ALS), a number of recent studies used terrestrial laser scanning (TLS) for the biomass estimation in spatially confined areas. One such instrument is the Echidna® Validation Instrument (EVI), which is configured to fully digitize the returned energy of an emitted laser pulse to establish a complete profile of the observed vegetation elements.

In this study we assess and compare a number of canopy metrics derived from airborne and terrestrial laser scanning. Three different experiments were conducted using discrete return ALS data and discrete and full waveform observations derived from the EVI. While considerable differences were found in the return distribution of both systems, ALS and TLS were both able to accurately determine canopy height (Δ Height < 2.5 m) and the vertical distribution of foliage and leaf area ($0.86>r^2> 0.90$, $p<0.01$). When using more spatially explicit approaches for modeling the biomass and volume throughout the stands, the differences between ALS and TLS observations were more

distinct; however, predictable patterns exist based upon sensor position and configuration.

Keywords: LiDAR, terrestrial LiDAR, canopy architecture, leaf area, canopy volume, Echidna, EVI, Fluxnet, full waveform LiDAR

1. Introduction

To support a large number of modeling applications, accurate estimates of vegetation structure are required including global scale assessments of vegetation growth (Cote et al., 2009; Peddle et al., 1999; Schaaf et al., 1994). While optical remote sensing techniques can provide phenological vegetation characteristics over large areas, the capacity of 2-dimensional measurements to determine canopy structure is limited. LiDAR measures the three-dimensional distribution of vegetation elements in the canopy directly and, as a result, is particularly well suited for describing structural vegetation properties including tree heights, biomass, and canopy volume (Lefsky et al., 2005a; Lefsky et al., 2002a; Lim et al., 2003; Næsset 1997; Parker et al., 2004b).

Most vegetation related LiDAR applications rely on airborne platforms for data acquisition, with measurements acquired at altitudes between 500 and 3000 m. The Geoscience Laser Altimeter System (GLAS) aboard the Ice, Cloud, and land Elevation (ICESat) satellite has been providing space-borne data since January 2003. The GLAS instrument was developed primarily to meet ice mapping objectives, with a vegetation mapping capacity as secondary to overall mission objectives (Zwally et al 2002). While not configured for vegetation characterization, the GLAS instrument has been used to characterize forest structure (Boudreau et al., 2008; Lefsky et al., 2005b; Pang et al., 2008). Lessons learned from the vegetation focused applications of GLAS data are informing the development of vegetation focused spaceborne sensor as part of NASA's DESDynI mission (Dubayah et al., 2008). Duncanson et al (2008) have explored the relationship between GLAS returns and higher density airborne measures found within the nominally 70 m GLAS footprint.

The limitations typically encountered regarding the capacity of airborne LiDAR to detect individual canopy elements are related to the spatial density of the laser returns, size of the LiDAR footprint, scan angle and instrument power (Lovell et al., 2003). As a result, airborne instruments often fail to observe significant aspects of the lower canopy and stem structure when these elements are obscured by the upper canopy. Additionally, the data collected from airborne LiDAR is less suited for characterizing the woody component of vegetation because the vertical projection of the stems contains only little information about their shape and volume (Lovell et al., 2003). These woody components, however, may contain a significant proportion of a stand's biomass.

As a complement to airborne measurements, a number of recent studies have used ground-based or terrestrial LiDAR systems (TLS), which describe canopy structure in a bottom-up rather than a top-down approach (Parker et al., 2004a; Strahler et al., 2008; Van der Zande et al., 2006; Welles and Cohen 1996). There are some fundamental differences in the way ALS and TLS can measure the distribution of foliage elements within a canopy. Firstly, according to the random media model (Poisson distribution) objects closer to the instrument are more likely to produce a measureable return. Consequently, ALS is likely to collect more detailed information about the upper canopy, while TLS is likely to provide a more detailed assessment of the lower canopy. Secondly, ALS sample almost exclusively at near nadir view angles thereby yielding a relatively homogeneous distribution of measurements per unit area. A ground-based system in contrast, features a radial perspective of observations with most laser returns originating from near the location of the instrument. As a result, under the assumption of zero interceptions, the shot density is inversely proportional to the square of the

distance from the instrument. As opposed to ALS, some terrestrial laser systems can describe vegetation structure at a number of different view angles (Cote et al., 2009; Jupp et al., 2008; Strahler et al., 2008), which is required to allow the analysis of canopy clumping effects and leaf angle distribution (Chen 1996; Chen and Cihlar 1995; Whitehead et al., 1990) and their impact on canopy metrics. Overall, the spatial resolution of TLS is generally much higher than that of ALS, especially in the vicinity of the plot center; the spatial range, however, is often limited to only a few hundred meters.

Most commercially available laser scanners operate as so called discrete return scanners (Wulder et al., 2008b). These systems typically record between 1 and 5 returns per outbound laser pulse. Each return represents a discrete object in the path of the beam (for instance a part of a forest canopy, understorey, and the ground), whose distance is represented by the time elapsed between emittance and return of the pulse. Typically, these discrete return systems feature a footprint size of 0.1 m to 2 m (Lim et al., 2003; Wulder et al., 2008b), and can achieve sub-meter accuracy of terrain surface heights (Blair et al., 1994; Lefsky et al., 2002b). Full waveform laser systems have been specifically designed for measuring vegetation (Jupp et al., 2005) and produce a fully digitized vertical profile of the returned energy of a given emitted laser pulse. The range resolution of a full waveform scanner is determined by time interval with which the sensor is able to record energy levels of an incoming waveform. The beam divergence varies with the instrument, but is generally larger than that of discrete waveform scanners.

A detailed understanding of the differences between airborne and ground-based, discrete return and full waveform LiDAR and the implications of these differences on the parameterization of canopy structure, will improve our understanding of the use of LiDAR as a tool for quantifying vegetation characteristics. For instance, a comparison of canopy parameters derived from ALS and TLS can inform on the robustness of individual modeling techniques with respect to the nature of its input observations. In this study, we compare and discuss the differences in a number of stand structural parameters measured by terrestrial and airborne LiDAR systems at a Douglas-fir (*Pseudotsuga menziesii* var *menziesii* (Mirb.) Franco) dominated research site in British Columbia, Canada. Ground-based LiDAR observations were acquired using the Echidna® validation instrument (EVI), a full waveform TLS, developed and built by the Commonwealth Scientific and Research Organization of Australia (CSIRO) (Jupp et al., 2008; Lovell et al., 2003; Strahler et al., 2008). The full waveform acquisitions were used to simulate discrete return TLS data by digitizing the ranges of the maxima of the returned waveforms. Full waveform and discrete terrestrial acquisitions were then compared to airborne LiDAR data acquired at the site.

2. Methods

2.1 Study area

The focus of this study is a 60 year-old coniferous forest on Vancouver Island, British Columbia, Canada, located at about 300 m above sea level (49°52’7.8” N, 125°20’6.3” W). The vegetation is second-growth, consisting of 80% Douglas-fir, 17% western red cedar (*Thuja plicata* Donn ex D. Don) and 3% western hemlock (*Tsuga heterophylla*

(Raf.) Sarg.) (Morgenstern et al., 2004). The understorey consists mainly of salal (*Gaultheria shallon* Pursh.), Oregon grape (*Berberis nervosa* Pursh.), vanilla-leaf deer foot (*Achlys triphylla* (Smith) DC), various ferns and mosses. The site is positioned at a northeast facing slope; the stand density is 1100 stems ha^{-1} with tree heights ranging between 30 and 35 m. Four 30 x 30m plots, all Douglas-fir dominated yet capturing a range of forest structural conditions, were measured within a radius of 5 km. The center position of each plot was approximated using a post-processed differentially corrected GPS with sub-meter accuracy; the plot corners were established using a measuring tape (distance) and a construction level (bearing).

2.2 Airborne LiDAR data acquisition

Discrete return airborne LiDAR data were acquired on August 14th 2008, using a Leica ALS50-II at a mean flying altitude of 2343 m. The sensor has a 150 kHZ pulse rate, recording up to 4 returns per outbound laser pulse. The estimated GPS accuracy of the sensor was 0.02, 0.03 and 0.05 m in East, North and height directions, respectively. When both ground and non-ground returns were considered, the dataset had an average density of 3.74 pts m^{-2}. The sensor's field of view was restricted to ± 15° off nadir and data were flown with average of 20% overlap between the flight lines. Flight and sensor parameters were optimized to achieve a ground return density of 0.5 m (after removal of canopy returns). Ground and non-ground returns were separated using a series of algorithms appropriate for the ground topography (Terrascan v 0.6, Terrasolid, Helsinki, Finland) (Kraus and Pfeifer 1999) and a DEM was generated from

the ground returns at a spatial resolution of 0.5 m (Fusion v 2.65, USDA, Forest Service).

2.3 Terrestrial LiDAR acquisition

While most currently available terrestrial laser scanners operate as discrete point systems, the EVI is configured to fully digitize the waveform of a scattered LiDAR pulse thereby allowing separation of scattering by trunks and other larger vegetation elements from scattering by leaves (Jupp and Lovell 2007). The EVI features a horizontally positioned laser that emits pulses at a wavelength of 1064 nm at a rate of 2 kHz. Pulses are directed toward a rotating mirror which is inclined at a 45° angle to the beam (Figure 1). The rotating mirror directs the beam in a vertical circle, which, coupled with a horizontal rotation of the tripod mounted instrument platform, results in a scanning motion that covers the upper and a significant part of the lower hemisphere of the scanner (Jupp et al., 2008; Strahler et al., 2008). The EVI beam is a fixed solid angle with a “top hat” energy profile which allows the energy density to be uniform over the (spreading) beam. The sampling was chosen so that at the horizontal scan there are no gaps between the volumes sounded by these beams. For higher zeniths the beams overlap and the data are not independent. This dependence can be taken out by processing and re-projection. Whilst the energy density reduces inversely to the second power of range, there are no gaps in the data.

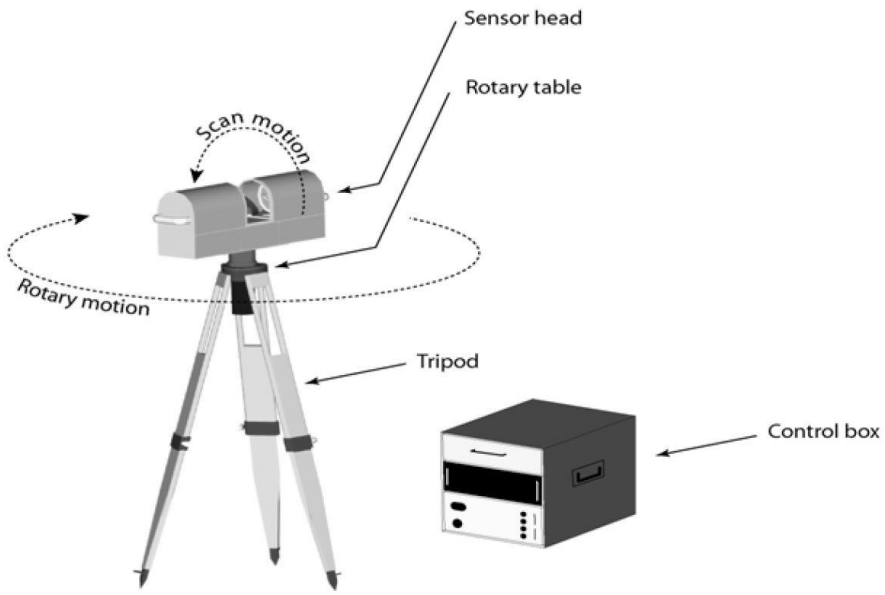

Figure 1: Schematic drawing of the Echidna® validation instrument (EVI, Figure adapted from Strahler et al., 2008)

EVI data were collected at the center and the four corners of each 30 x 30 m plot location using an angular sampling interval of 4 mrad and a beam divergence of 5 mrad to ensure some sidelap between individual acquisitions. The recordable range of the instrument is adjustable and was set to 120 m; the height of the instrument varied between 1.7 m and 1.9 m above ground, depending on the individual setup at each plot. Additional steps for EVI data processing have been described in detail elsewhere (Jupp et al., 2008; Jupp and Lovell, 2007; Strahler et al., 2008). Briefly, the recorded pulse energy of a reflected beam depends on the shape and orientation of the target, its distance to the instrument (range) and the basic reflectance at the wavelength of the laser (Strahler et al., 2008). As a result, the apparent reflectance (that is, the reflectance that a large, flat, lambertian and opaque target normal to the laser beam would have, to return the observed power at the specific range) of a targeted surface is given by (Jupp et al., 2008)

——— (1)

where is the mean phase function for the varying facets of a target, is the angle relative to the facet normal, g is the distribution function for the facet directions, is the normal reflectance of a facet and is the probability of a gap between the instrument and the target (Jupp et al., 2008). The hit probability at a given range (———), the normal reflectance of the objects at this range and their scattering phase function depend on the orientation and specularity of the targeted object (Jupp et al., 2008).

Discrete point observations may be simulated from full waveform acquisitions by using filtering and first and second derivatives to locate the peaks in EVI shots as a point cloud (Jupp and Lovell 2007). Discrete point data were digitized for all observations made at a zenith angle <130˚. The noise threshold was set to 0.1 % reflectance.

2.4 Combination of multiple scanning locations

Due to the radial perspective of the TLS results less laser energy is available to illuminate objects at greater ranges from the instrument. In addition, occlusion of far objects by those closer to the instrument further decreases the likelihood of returns with increasing distance (Hilker et al., 2009). One possible means to minimize these effects is to combine TLS data from multiple locations within a plot area to observe vegetation from different view angles, minimize shading effects and provide a more homogenous distribution of observation points within a plot. For instance, Hilker et al., (2009) combined discrete return data collected at the center and the 4 corner locations of each

of the described 30 x 30 m plots (Figure 2) using artificial, highly reflective reference targets (Polystyrene balls, Ø 20 cm) as tie-points to establish a relative orientation between the individual data acquisitions. The Polystyrene balls were placed within each plot prior to data collection so that they were visible from all five scanning locations (Figure 2). A simple thresholding technique of the reflected laser energy was then used to automatically identify these tie-points within each TLS dataset. The LiDAR hits which were recorded in local coordinates at each scanning location were then converted into a common reference system by means of a Helmert transformation. This approach effectively minimized occlusion within the 30 x 30m plot areas, thereby yielding point densities of > 300 hits/m^2 for >90% of the area under investigation (Hilker et al., 2009). The technique also allowed the generation of accurate digital elevation models (DEM) for each plot from discrete EVI data by extracting the minimum elevations from the merged TLS point cloud using a spatially moving boxcar filter of 0.5 m dimensions (see Hilker et al., 2009 for details).

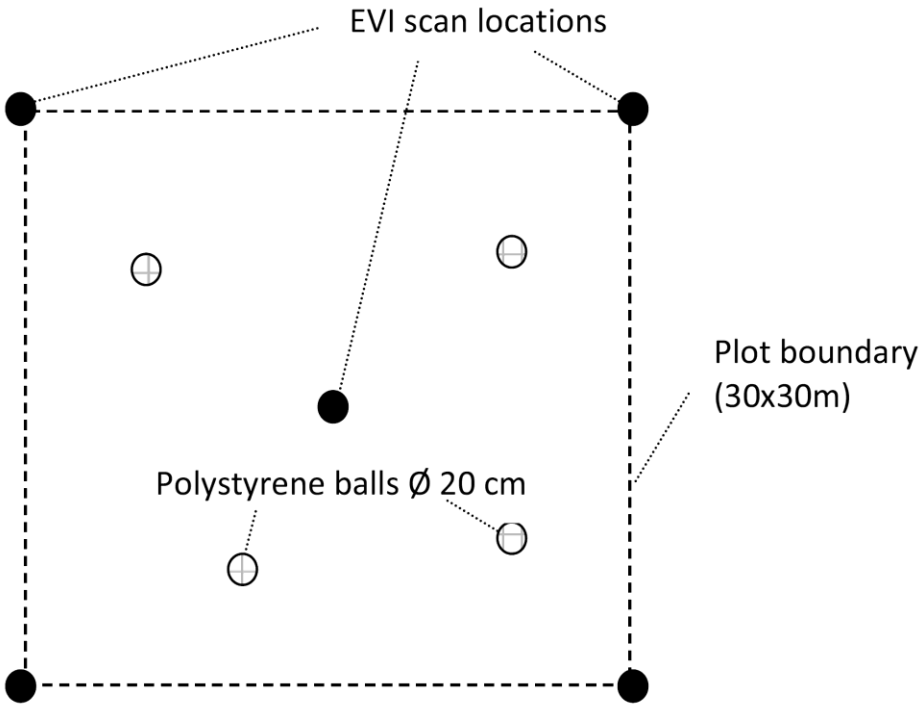

Figure 2: Plot setup at the Douglas-fir dominated study site. A total of four 30 x 30 m plots were established with EVI scans located at the four corners and the center of each plot. Highly reflective Polystyrene balls which were placed on metal stakes were used to establish a relative orientation between the individual scan locations (Hilker et al., 2009)

While this method can easily be applied to discrete return observations, it is less applicable to full waveform data. First, individual canopy elements may be misrepresented when simply adding or averaging observed apparent reflectance measurements from multiple scanning locations, as the facet of an observed target depends on the position of the observer. Second, full waveform observations are often stored in data cubes, which made the combination of multiple datasets difficult.

2.5 Approach

We compared the canopy metrics derived from three different types of LiDAR observations: First, structural stand characteristics were derived from discrete ALS observations. Second, discrete return TLS data were simulated from full waveform EVI observations by locating the energy maxima. The point data from the center and the four corner locations of each plot were then combined to allow a better representation of the investigated plots. Finally, canopy characteristics were also derived from individual, full waveform acquisitions and then converted to plot level data by averaging the metrics derived at each of the five scanning locations per plot.

2.6 Canopy heights

The average canopy height for the top 40, 30, 20 and 10% of all LiDAR returns was determined for each plot from discrete airborne and terrestrial LiDAR data, respectively. The dominant stand height was also calculated using a spatial stratification approach that divides each plot into four smaller grid cells for which the highest return was extracted and averaged with the highest return of the other grid cells (Næsset 1997). Finally, the maximum canopy height, defined as the highest LiDAR return per plot, was determined from airborne and terrestrial laser data.

2.7 Canopy profiles and leaf area

One of the most commonly applied measures of canopy architecture is the leaf area index (L), defined as half the total foliage area per unit ground surface area (Chen and

Black 1992). L can be indirectly determined from LiDAR by estimating the probability of gap in the canopy ( ) (Jonckheere et al., 2004; Jupp et al., 2008), defined as (Chen 1996)

(2)

where θ is the view zenith angle and $G(\theta)$ is the Ross-G function describing the mean area projection of plant elements in the direction θ. Often, a random orientation of foliage is assumed for needle leaf forests, and, as a result, $G(\theta)$ may be approximated using a constant of 0.5 (Chen et al., 1997; Chen 1996). L(z) is the cumulative leaf area from the ground to a given height z. For a terrestrial LiDAR system which scans the hemisphere above the instrument at multiple angles, the total (effective) leaf area L is the integral of measurements taken at all θ (Miller et al., 1964, 1967, Jupp et al., 2008)

(3)

The foliage profile Fp(z), defined as the vertical distribution of phytoelement density above the ground (Ross 1981; Warren Wilson 1965), is the 1st derivative of L(z) (Lovell et al., 2003). Due to the inability of airborne LiDAR systems to observe the canopy under multiple view angles, airborne LiDAR is incapable of resolving foliage angle distribution and canopy clumping and as a result, the profiles derived from airborne LiDAR are often referred to as “apparent” foliage profiles Fp(z)’ (Lovell et al., 2003). The differences between actual and apparent foliage profile are discussed in detail in (Ni-Meister et al., 2001).

The determination of from full waveform EVI data has been discussed in detail by Jupp et al. (2008). For a given range and zenith, is given as:

(4)

where is the apparent reflectance measured at a time t, T' is ct/2 and r is the range to which the gap probability is taken.

When using discrete return LiDAR, the probability of canopy gap can be estimated as the sum of the total number of hits down to a height z, relative to the total number of independent LiDAR shots (N) (Coops et al., 2007; Lovell et al., 2003; Riano et al., 2003):

$$P_{gap}(z)' = \frac{1 - \sum_{z=j}^{z=z_{max}} \#z_j}{N} \quad (5)$$

where #z is the number of hits down to a height z above the ground (or the range to which the gap probability is taken). The dash indicates the apparent nature of P_{gap}. Assuming θ=0°, L(z)' then becomes (Lovell et al., 2003),

(6)

and FP (z)' is the first derivative of L(z)'.

In this study, foliage profiles and leaf area were determined in three different ways from LiDAR. First, FP(z)' and L(z)' were calculated from airborne using the discrete point clouds. Second, FP(z)' and L(z)' were also calculated from terrestrial LiDAR using the

simulated discrete point data. Third, FP(z) and L(z) were calculated from the full waveform EVI observations.

The total leaf area per plot was also determined from hemispherical photography using a fisheye-lens. The camera was located on a tripod at the center and the four corner locations of each plot (coincident to the EVI measurements) and data were analyzed using the Gap Light Analyzer software (Frazer et al., 2001).

2.8 Canopy volumes

Canopy volume models (CVM) (Lefsky et al., 1999) characterize the three dimensional structure of a forest canopy by quantifying the differences in the total volume and spatial organization of the tree foliage. CVMs organize the canopy space as a matrix composed of three dimensional grid cells or voxels. These voxels are classified as either "filled" or "empty" depending on the level of energy (that was reflected from that space in the canopy (Lefsky et al., 1999). An “empty” voxel can be located either below (“closed gap”) or above the canopy (“open gap”), whereas a “filled” voxel is labelled either “euphotic”, if the cell is located within an uppermost percentile (65%) of all filled grid cells of that column, or "oligophotic" if the voxel is located below this point in the profile (Coops et al., 2007; Richards 1983). This method provides a broad classification approach to divide the canopy into photosynthetically active and less active zones. The 65% threshold value was derived from a theoretical expectation about the fraction of energy returned from the first layer of leaves, when assuming a light extinction coefficient of one (Lefsky et al., 1999).

Originally developed for full waveform airborne LiDAR observations (Lefsky et al., 1999), CVMs have since been adapted to be used also with discrete return data (Coops et al., 2007). Lefsky et al (1999) used voxel sizes of 10 x 10 (horizontal) x 1 m (vertical) to account for the relatively coarse spatial resolution of the airborne LiDAR data. In this study, the voxel size has been adapted to accommodate the much higher point density of TLS data by changing the size of the superimposed grid to include approximately the same number of observations for airborne and terrestrial LiDAR. The voxel size chosen for the discrete airborne observations was 36 m^3 (6 x 6 x 1 m), the resolution selected for discrete and full waveform terrestrial data was 1 m^3 (1 x 1x 1 m).

3. Results

Figure 3A-B illustrates the differences between the point cloud generated from the discrete airborne LiDAR, the simulated EVI point clouds and the full waveforms observed from the terrestrial laser scanner. Figure 3A shows the discrete airborne data superimposed on the EVI generated point cloud. The upper canopy was well characterized by airborne LiDAR with shapes of individual tree crowns being represented in the dataset; only relatively few measurements, however, originated from lower parts in the canopy. The terrestrial observations (smaller green dots), showed a much higher level detail of the recorded scene, with point clusters representing individual stems, branches and understorey vegetation. This dataset, however, seemed to less well represent the topmost part of the canopy and estimates of tree heights were generally lower than those of the airborne LiDAR data. Figure 3B shows the full waveform EVI data up to the recorded range of 120 m distance (mean reflectance of an

individual scan shown). The distortion is due to the representation of the y dimension as zenith angle. As opposed to the observations shown in Figure 3A, the full waveform observations provided a complete three dimensional image of the observed forest stand.

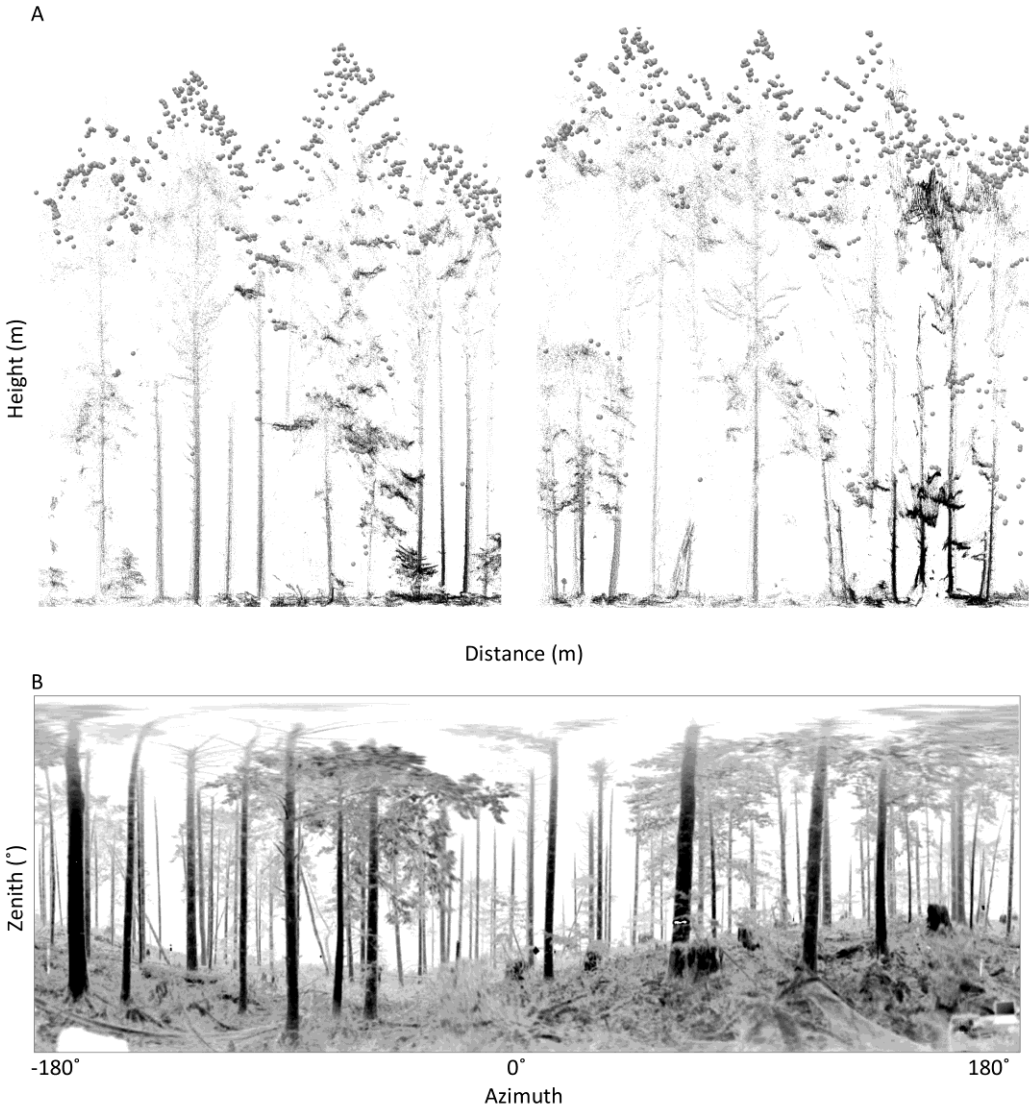

Figure 3A: Comparison between discrete return airborne and terrestrial LiDAR. The airborne dataset is shown as white dots, the smaller green dots represent the combined and discrete terrestrial data. The terrestrial observations (smaller green dots), showed a much higher level detail of the recorded scene, with point clusters representing individual stems, branches and understorey vegetation. Figure 3B: Full waveform representation of an individual EVI scan. The tree tops are distorted in this representation due to the projection of hemispherical observations onto a two-dimensional plane (Andrieu Transpose projection). For illustration purposes, the mean waveform is shown in this figure

The return densities per unit canopy space for airborne and terrestrial LiDAR observations are illustrated in Figure 4 using plot 1 as an example. Figure 4A shows the mean hit density of the airborne LiDAR data; the hit distribution of the combined TLS returns is shown in Figure 4B. The average number of LiDAR returns was 0.2 hits m^{-3} for the airborne data and 25.5 hits m^{-3} in case of the terrestrial observations. Over 75% of all airborne LiDAR returns originated from the top 10 m of the tree canopy, while the combined TLS data showed a more homogeneous distribution of hits as 75% of the discrete and combined TLS returns covered about 26 m of tree canopy. Figure 4C shows the returned energy levels (in % reflectance per area) of the full waveform observations (only the center plot is shown). The x-axis represents the horizontal distance from the scanning instrument (up to 50 m); the y-axis shows the azimuth of the observation. The returned energy levels revealed a steep gradient towards the center of the scan as 75% of the emitted waveform energy was reflected within the first 18 m horizontal distance from the observing EVI.

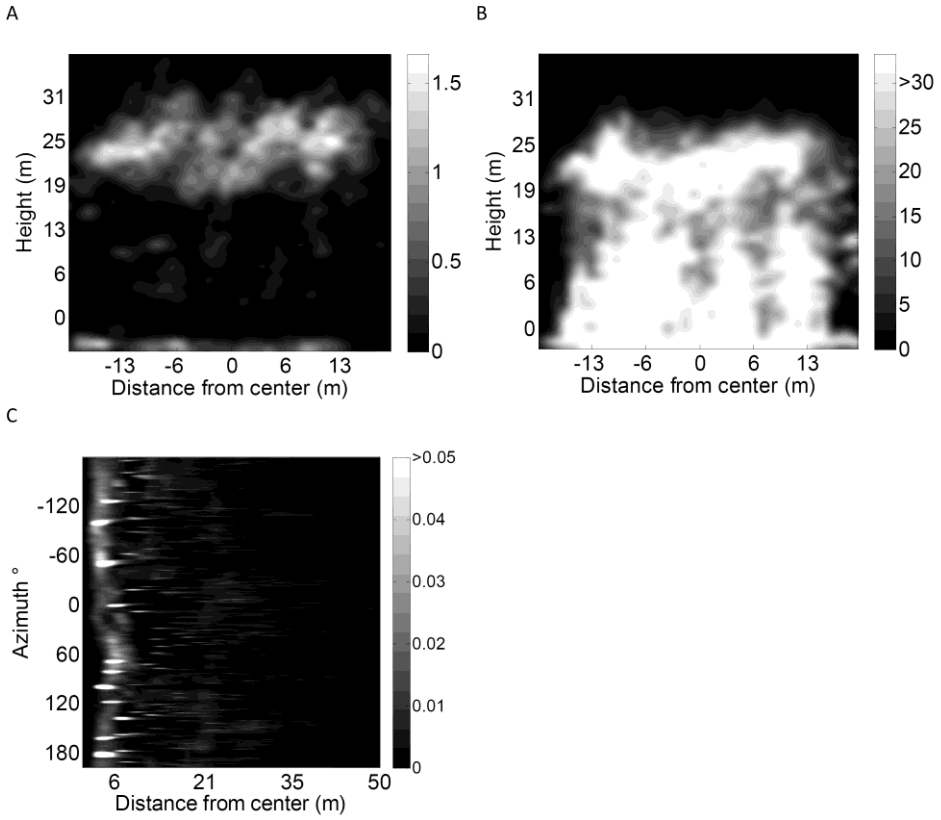

Figure 4A-C: Hit density of discrete airborne (A), discrete and combined terrestrial (B) and full waveform terrestrial (C) data. The grey levels in Figures A and B represent the total number of returns per m^3, where as the grey levels in Figure C correspond to the mean energy (in % of the outbound laser energy) reflected at this azimuth and range.

A comparison between various canopy height estimates (four height percentiles (top 40%, top 30%, top 20% and top 10% of all LiDAR returns), maximum and dominant stand height) derived from discrete airborne and ground-based LiDAR is given in Figure 5. While TLS and ALS data showed good agreement between dominant and maximum stand heights, the height percentiles measured by TLS were, on average, between 14.2 m (in case of the top 40 % height) and 9.6 m (in case of the top 10 % height) lower than those of the airborne measurements.

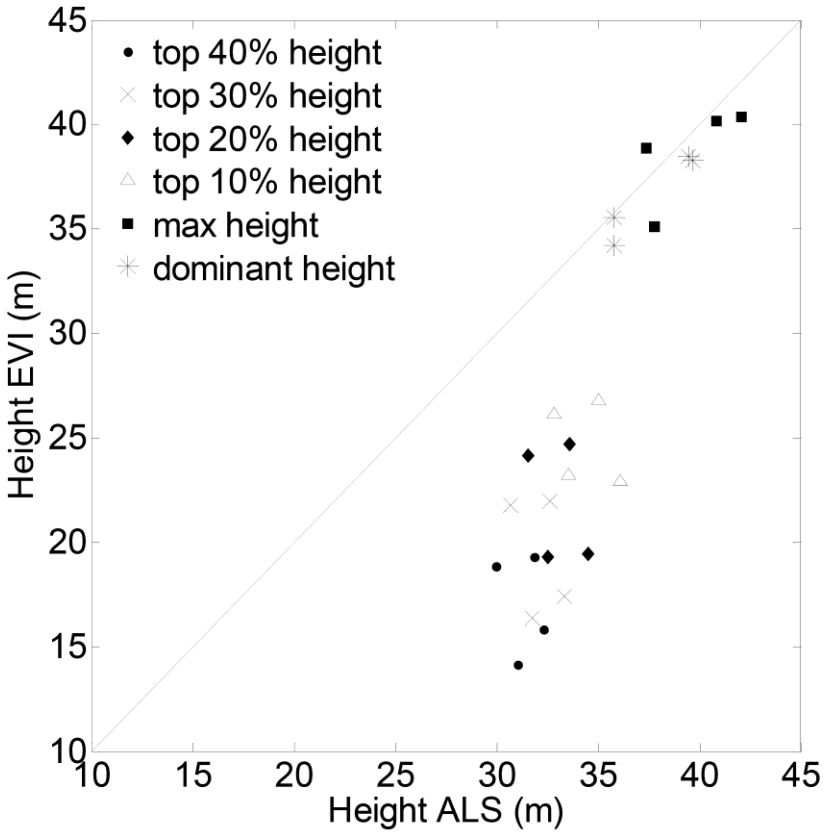

Figure 5: Comparison between the top 40%, top 30%, top 20% and top 10% height percentiles and maximum and dominant stand height derived from discrete ALS and TLS. The diagonal line represents the 1:1 line.

Figure 6 shows the apparent foliage profiles derived from discrete return ALS and TLS and the actual foliage profile determined using full waveform TLS data. The figure numbers A-D correspond to the plot numbers 1-4. The apparent foliage profiles of the discrete TLS data were highly correlated to those estimated from ALS (r^2 = 0.86, 0.66, 0.82, 0.90, $p<0.01$ for plot 1-4, respectively). Please note that the r^2 values presented here only have a local descriptive meaning due to some expected autocorrelation in the dataset. On average, best agreement between Fp'_{TLS} and Fp'_{ALS} was found in the upper part (z>20 m) of the canopy (^{2}= 0.87, $p<0.01$), while Fp'_{TLS} and Fp'_{ALS} were less well correlated in the lower (z<20 m) canopy (^{2} = 0.48, $p<0.01$). Fp_{TLS} was closely

correlated to the apparent foliage profiles determined from ALS and TLS data. The coefficients of determination for the relationship between Fp'_{TLS} and Fp_{TLS} were r^2=0.91, 0.85, 0.66, 0.90 ($p<0.01$) for plot 1-4, respectively, those for the relationships between Fp'_{ALS} and Fp_{TLS} were r^2=0.88, 0.66, 0.75, 0.92 ($p<0.01$), respectively. While Fp_{TLS} followed the general shape of the apparent foliage profiles closely, its appearance was smoother as observations were integrated over a large number of zenith angles. The apparent and actual foliage profiles of plot 3 (Figure 6C) differed notably from those of the other plots due to a larger wind throw and upcoming succession near the plot center.

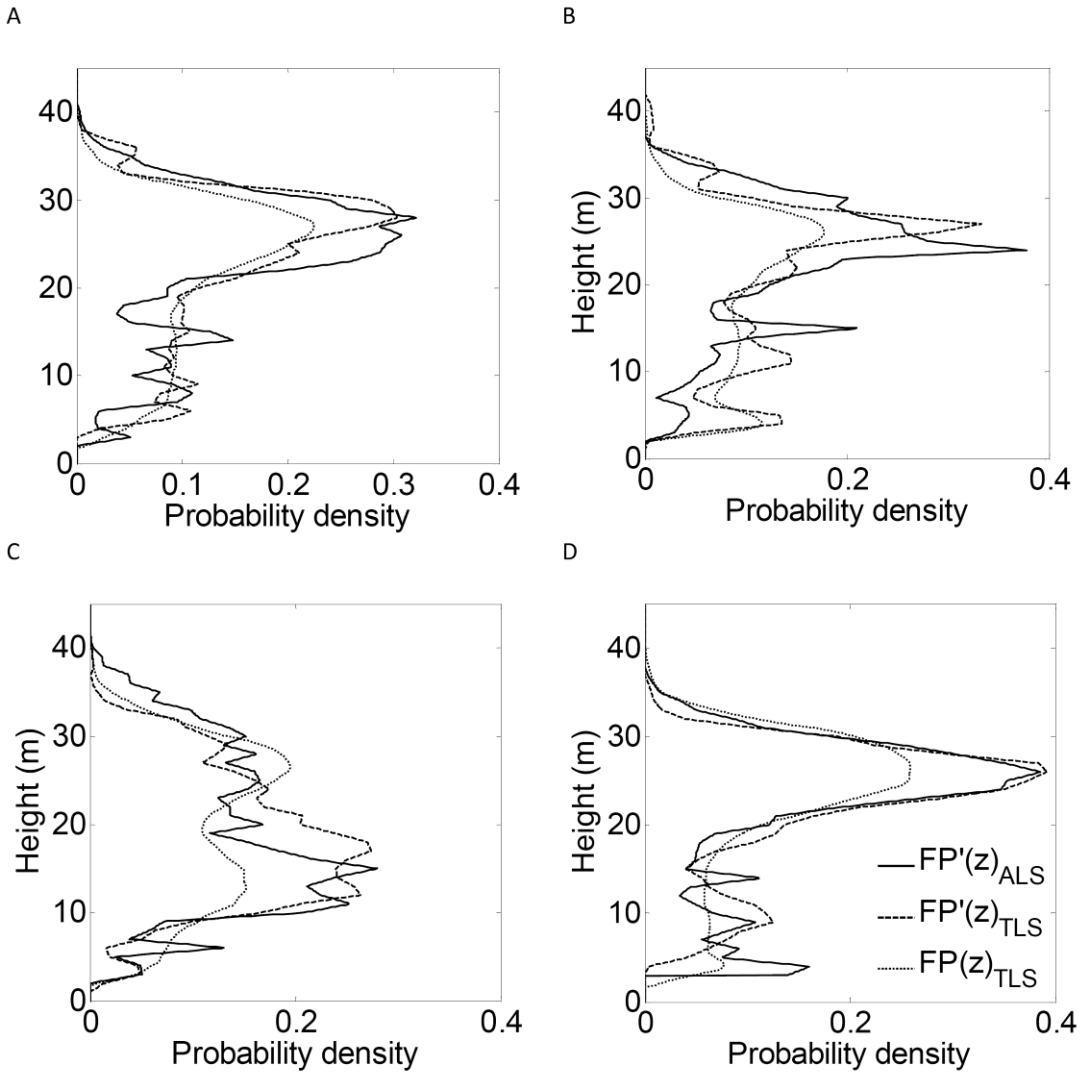

Figure 6A-D. Apparent and actual foliage profiles derived from discrete return ALS and TLS full waveform TLS, respectively. Figure 6 A-D correspond to the plot numbers 1-4. FP' of the discrete TLS data were highly correlated to those estimated from ALS (r^2 = 0.86 (A), 0.66 (B), 0.82(C), 0.90 (D), p<0.01), the relationships between

Figure 7A-D shows a comparison of the LAI profiles (L_E) determined from airborne and terrestrial LiDAR observations, the figure numbers A-D correspond to plot numbers 1-4. Similar to Figure 6, L_E has been estimated for airborne and terrestrial discrete return observations and full waveform TLS data. The discrete ALS and TLS observations showed a good agreement of total LAI values, some differences, however, were

observed in the lower canopy as the LAI estimated from the TLS generated point cloud showed slightly larger values than those of the airborne data. The full waveform estimates of L_E were, on average, higher than those obtained from the discrete point data, particularly in the lower half of the canopy.

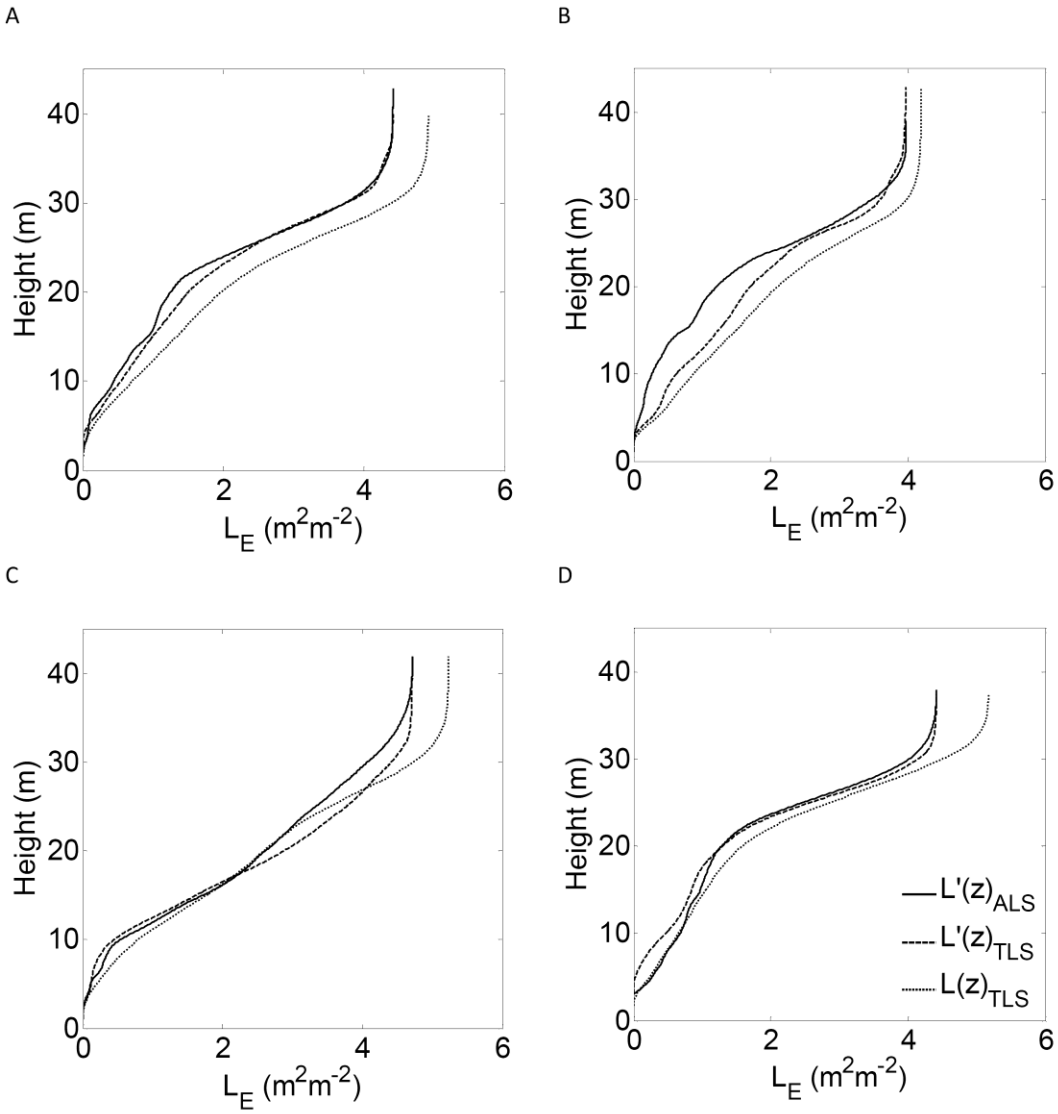

Figure 7A-D. Leaf area profiles derived from discrete return ALS and TLS full waveform TLS, respectively. Figure 7 A-D correspond to the plot numbers 1-4.

Figure 8 shows the relationship between total leaf area obtained from full waveform TLS data (L_{TLS}) and leaf area observed from hemispherical photography (L_{Hemi}). To allow a direct comparison between EVI and photographic data, individual EVI observations rather than the merged, plot level TLS data were used. Figure 8A presents LAI estimates from L_{TLS} and L_{Hemi} using all observations up to a zenith angle of $\theta \leq 75°$. Figure 8B shows the LAI estimates for the same plots using observations up to a zenith angle of $\theta \leq 60°$. A highly significant relationship ($p<0.01$) was found between L_{TLS} and L_{Hemi} (Figure 8A-B), the model was, however, biased as the camera measured significantly lower LAI values throughout the study area. Figure 9 shows the relationship between L_{TLS} and L_{Hemi} stratified by zenith angles. The location on the x-axes shows the center zenith angle of a stratum ($5°< \theta \leq 10°$, $10°< \theta \leq 15°$, … , $50°< \theta \leq 55°$), the y-axis describes the coefficient of determination for the relationship between LiDAR estimated and photographical LAI. The relationships between L_{TLS} and L_{Hemi} were moderate for smaller zenith angles but increased for observations made lower in the canopy. The r^2 values ranged between 0.31 ($15°< \theta \leq 30°$) and 0.76 ($50°< \theta \leq 55°$) ($p<0.01$).

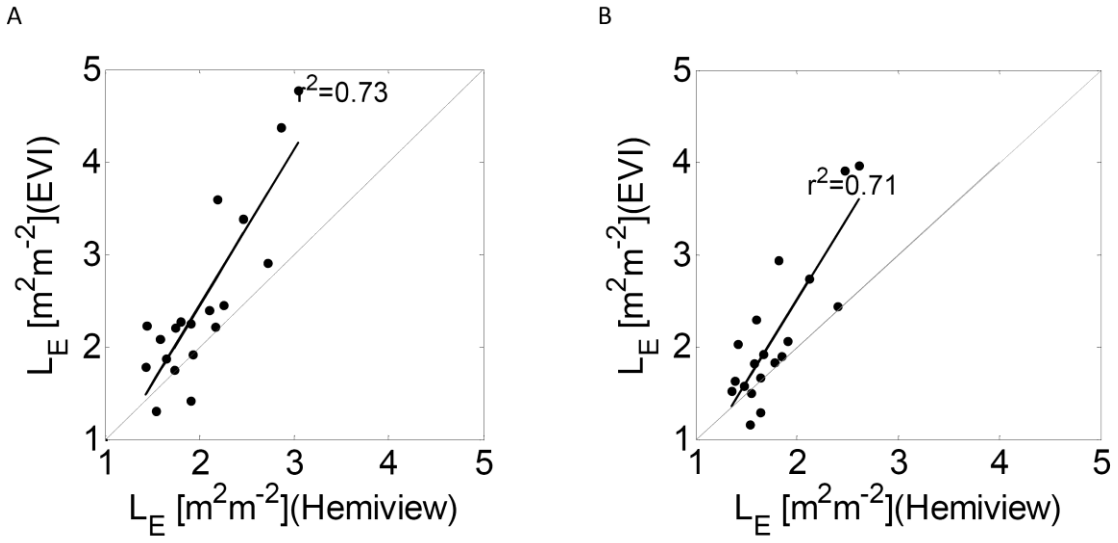

Figure 8. Relationship between total leaf area obtained from full waveform TLS data (L_{TLS}) and leaf area observed from hemispherical photography (L_{Hemi}). Figure 8A represents LAI estimates from L_{TLS} and L_{Hemi} using all observations up to a zenith angle of θ ≤ 75°. Figure 8B shows the LAI estimates using observations up to a zenith angle of θ ≤ 60°.

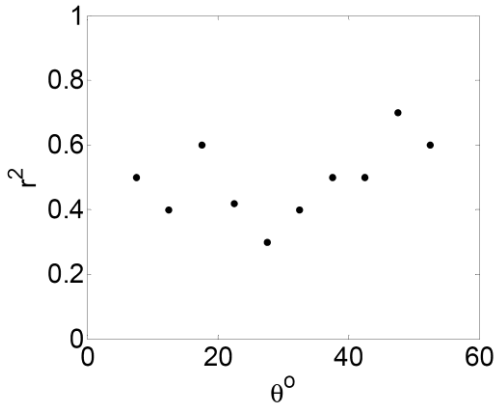

Figure 9: Coefficient of determination (p<0.01) for the relationship between L_{TLS} and L_{Hemi} stratified by zenith angles. The location on the x-axes shows the center zenith angle of a stratum (5°< θ ≤ 10°, 10°< θ ≤ 15°, … , 50°< θ ≤ 55°), the y-axis describes the coefficient of determination for the relationship between LiDAR estimated and photographical LAI.

Figure 10 shows the results of the canopy volume models for the discrete airborne (left column), the discrete TLS point clouds (central column) and the full waveform TLS observations (right column). The rows correspond to plot 1-4. The black color corresponds to the % volume of closed canopy gap per height level, dark grey

represents the shaded (oligophotic zone) canopy volume and the lighter grey area describes the more photosynthetically active part of the canopy (euphotic zone). The lowest amount of euphotic canopy has been estimated from the airborne data (left column), whereas significantly larger amounts of canopy volume where found to be within the topmost 60% of the TLS observations (center and right column). Additionally, the algorithm predicted a larger amount of below canopy gaps when using the airborne data rather than discrete EVI observations, particularly in the lower half ($z<20$ m). This part of the canopy is partially obscured to airborne observations by canopy elements from above. The top tree heights (that is, the topmost recorded canopy element) showed good agreement between the two discrete datasets; however, a much larger percentage of the total volume was, recorded by the airborne data in the upper 30 to 40 m of the canopy. The full waveform TLS observations showed the greatest canopy volume in the upper portion of the canopy. Additionally, the amount of canopy gap was significantly larger that those estimated from the discrete return data.

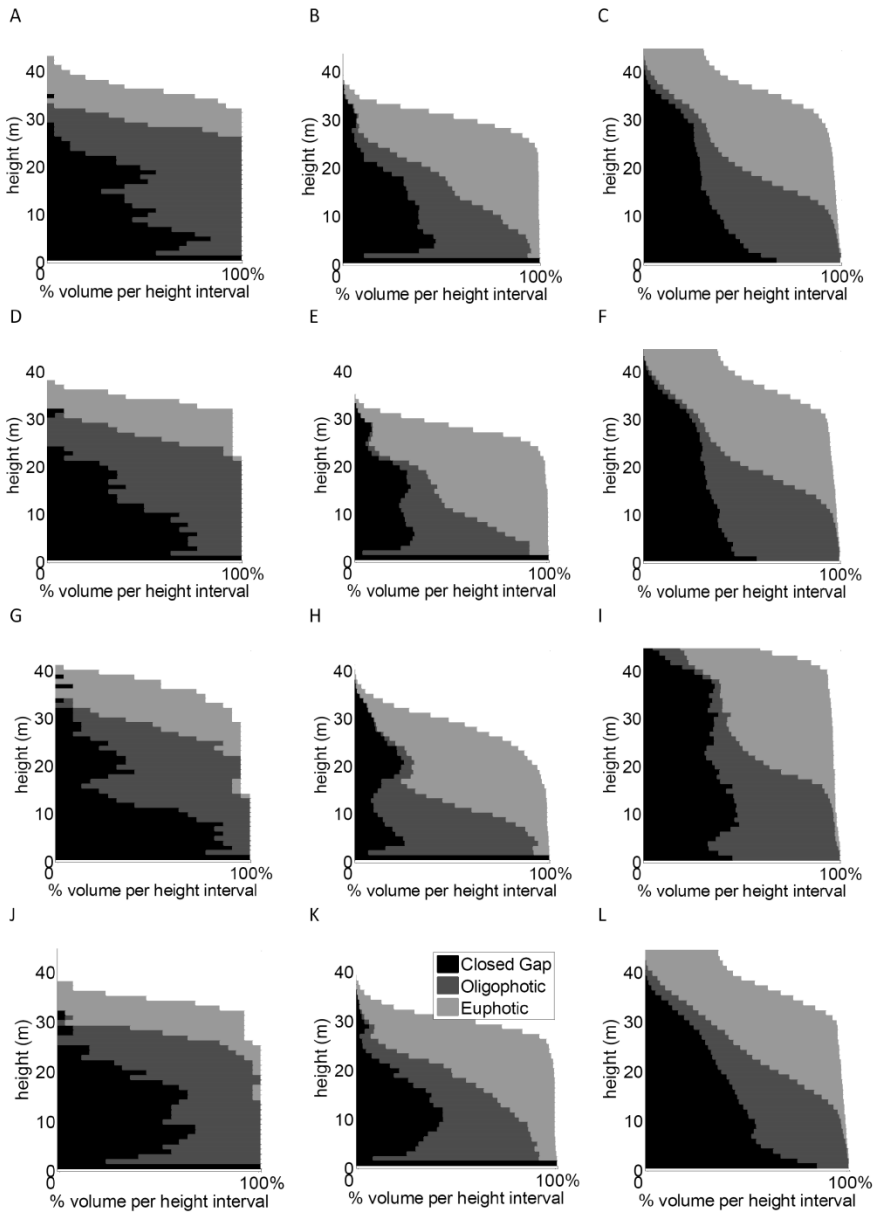

Figure 10: Canopy volume models (CVMs) for the discrete airborne (left column), the discrete TLS point clouds (central column) and the full waveform TLS observations (right column). The rows correspond to plot numbers plot 1-4. The black color corresponds to the % volume of closed canopy gap per height level, dark grey represents the shaded (oligophotic zone) canopy volume and the lighter grey area describes the more photosynthetically active part of the canopy (euphotic zone).

4. Discussion

The increased ability of the discrete and full waveform TLS observations to penetrate the forest canopy demonstrated the potential of TLS data for characterizing understorey vegetation and the below canopy architecture in the examined Douglas-fir forest (Figure 3). In contrast, the airborne observations largely described the top canopy layer, whereas the elements in the lower canopy were illustrated with less detail. Similar results on the distribution of terrestrial and airborne LiDAR returns have previously been reported (Chasmer et al., 2004). The results found in figure 3 are also confirmed by the findings in Figure 4 illustrating the distribution of hit densities and return energies throughout plot 1. When comparing the vertical distribution of points, the EVI covered, on average, a greater detail with return densities considerably exceeding those of the airborne data (Figure 4B). A comparison between Figure 4B and 4C demonstrates the usefulness of combining discrete TLS observations from multiple scanning locations to obtain full coverage of the examined plots (Hilker et al., 2009). For instance, 75% of the returned energy of individual TLS observations (Figure 4C) originated from within the first 18 meters of the instrument and, as a result, objects closer to the instrument are better characterized than those that are located further away from it. This effect needs to be considered when comparing individual TLS observations to other plot level measurements as errors due to spatial mismatch may occur, at least when these other observations are spatially explicit. In contrast, the combined dataset (Figure 4B) yielded a much more homogeneous horizontal distribution of points throughout the plot making the data more comparable and representative for the entire plot. It should, however, be noted that converting full waveform information to discrete point clouds (which is

required in order to be able to combine multiple data sets) also means a loss of information for instance about the statistics of volumes. One of the biggest unknown when using a discrete point representation (which limits its accumulation into voxels) is whether a gap exists within a given space because of the absence of objects (such as branches, leaves etc.) or because the laser beam does not reach the required volume. Even when combining multiple TLS data sets there may still be volumes that are not “illuminated” by any of the scans. This limitation needs to be taken into consideration when evaluating canopy statistics from discrete observations.

The effects of different point distributions on height measurements derived from LiDAR were demonstrated in Figure 5. TLS and ALS data showed very good agreement for dominant and top canopy height, thereby demonstrating that TLS observations can be used to accurately determine tree and stand height. The deviations found when comparing height percentiles of the ground based and airborne data acquisition were predictable as they consistently increased with the percentile used (Figure 5). The larger range of heights observed for the different percentiles from TLS compared to ALS again demonstrates the greater ability of these data to penetrate the examined canopy, as hits were more evenly distributed throughout the vertical canopy layers. The effect is expected to be less significant in more open canopies which have a higher probability of airborne data reaching lower elements in the canopy.

While the distribution of canopy hits was considerably different for the examined datasets, good agreement was found between the estimates of foliage and leaf area distribution from airborne and terrestrial LiDAR (Figure 6, Figure 7). This is an important result as it shows the capacity of both ALS and TLS to accurately determine the

arrangement of foliage despite the differences in the distribution of LiDAR returns. Similar findings have previously been reported by Lovell et al. (2003) who found good agreement between ground measured and airborne foliage profiles in a number of different forest stands in south-eastern Australia. In case of the discrete return data, the canopy profile (and hence the LAI profile) is driven by the ratio of returns originating from the main crown layer and the total number of independent LiDAR shots (eqn. 5). This relation effectively normalizes the observations with respect to the hit density as a larger number of shots will also increase the probability of a hit at a given height level. A similar effect can be observed for the full waveform data where individual energy levels are related to the outgoing pulse energy (eqn. 4). While the probability densities in the upper canopy layer were very similar for discrete return ALS and TLS data, certain differences were found in the lower part of the canopy. For instance, the probability densities of airborne LiDAR within the lower 20 m of the canopy were, on average, smaller than those of the ground based measurements and, as a result, the area underneath those graphs (which corresponds to the LAI) was slightly higher in the lower canopy (Figure 7). The full waveform integrated canopy profiles appeared, on average, smoother than those obtained from discrete return data. This is likely due to the integration of profiles over a large number of zenith angles. Overall, a highly significant relationship was found between the canopy profiles obtained from individual full waveform measurements and those observed using the combined point clouds. The plot level results shown in Figure 6 and 7 are not spatially explicit and it can be concluded that the canopy distribution was well represented by the individual sweeps observed by the EVI.

The significant correlation found between the hemispherical photographs and the TLS observations demonstrated the value of the TLS observations to measure leaf area, however, only moderate correlations were found between the observations made at specific zenith angles. Slightly higher correlations have previously been reported by Lovell et al (2003) for the Australian forest site. As in the case of Lovell et al., (2003), the hemispherical canopy photographs in this study had to be collected over multiple days (for practical reasons) and, as a result, the sun position varied throughout the observation period, as did cloudiness the site. Consequently, the conditions for collecting the photographical observations in this study were not optimal, which may explain some of the variation observed in Figure 8 and 9. The apparent lack of gaps for high zeniths in hemispherical photographs is probably more realistic than true gaps to a fixed range detected by EVI, realistic estimates of LAI from either dataset should not use data of more than about 70 degrees zenith (Lovell et al., 2003). As a result of the three dimensional nature of the EVI data, TLS based LiDAR is able to yield information beyond that which can be obtained from hemispherical photographs (Jupp et al., 2008). Consistent with findings by other authors (Hopkinson and Chasmer 2009), the cover observed by hemispherical photographs in this study was lower than that estimated from LiDAR.

The most notable differences were observed between the canopy volume estimates derived from ALS and discrete and full waveform TLS. When comparing airborne and terrestrial discrete return observation, a larger amount of below canopy gap was found for the ALS data. This finding is consistent with Lovell et al., (2003) and demonstrates the difficulties of obtaining accurate below canopy biomass estimates from airborne

laser scanning. Specifically, the step gradient in return densities towards the lower portion of the canopy is likely to result in a underestimation of understorey vegetation as the sparse distribution of ALS returns is less suited to characterize the volume of stems biomass and smaller trees (Jupp et al., 2008; Lovell et al., 2003; Strahler et al., 2008). The differences observed in the euphotic and oligophotic canopy volume of the left and the central column in Figure 10 again reflects in the fundamental differences in the vertical distribution of LiDAR returns demonstrated in Figure 4. Importantly, as opposed to the foliage profiles and LAI estimates shown in Figure 6 and 7, the CVM technique (Coops et al., 2007; Lefsky et al., 1999) is spatially explicit as it divides the canopy space into voxels and then compares the classification result of each voxel with those of the voxels above. This also explains why the results shown for the full waveform TLS data are fundamentally different from those given for the ALS and discrete return TLS data. First, the reduction of radial full waveform information to point data, which are located at centre of a given beam, leads to an over-representation of the canopy space above the EVI, because this space will contain higher return densities than the identical volume at the same distance in any vertical direction (see also Figure 3B compared to Figure 4C). Second, the volume of below canopy gaps predicted by these individual measurements is likely to be overestimated due to the occlusion effect by other vegetation elements discussed above (Hilker et al., 2009).

5. Conclusion

The results of this study have shown that ground based LiDAR measurements can be a valuable addition or alternative to airborne LiDAR observations depending on the

information need being addressed. While fundamental differences exist in the way ground based and airborne LiDAR returns are distributed throughout the canopy, plot level estimates of leaf area, foliage profile and dominant and maximum canopy height were highly correlated to those derived from airborne measurements. The combination of multiple terrestrial LiDAR observations from different locations can be a useful technique for overcoming limitations inherent to the radial perspective of TLS and may result in more realistic estimates when characterizing the below canopy biomass in a spatially explicit mode.

Acknowledgements

Past and current members of the Integrated Remote Sensing Studio, Faculty of Forest Research management, University of British Columbia are thanked for their assistance with the field work. This work is partially funded by an NSERC Discovery grant to Coops. Additional funding support was also received from the Canadian Wood Fibre Centre, of the Canadian Forest Service of Natural Resources Canada.

References

Blair J, Coyle D, Bufton J, Harding D (1994) Optimization of an airborne laser altimeter for remote sensing of vegetation and tree canopies. vol II, pp 939-941

Boudreau J, Nelson RF, Margolis HA, Beaudoin A, Guindon L, Kimes DS (2008) Regional aboveground forest biomass using airborne and spaceborne LiDAR in Quebec. Remote Sensing of Environment 112: 3876-3890

Chasmer L, Hopkinson C, Treitz P (2004) Assessing the 3D frequency distribution of airborne and ground-based LiDAR data for red pine and mixed deciduous plots. ISPRS Workshop Laser-Scanners for Forest and Landscape Assessment, Freiburg, Germany, pp 66-70

Chen J, Black T (1992) Defining leaf area index for non-flat leaves. Plant, cell, and Environment 15: 421-429

Chen J, Rich P, Gower S, Norman J, Plummer S (1997) Leaf area index of boreal forests: Theory, techniques, and measurements. Journal of Geophysical Research 102: 29 429-429 443

Chen JM (1996) Canopy Architecture and Remote Sensing of the Fraction of Photosynthetically Active Radiation Absorbed by Boreal Conifer Forests. Ieee Transactions on Geoscience and Remote Sensing 34: 1353-1368

Chen JM, Cihlar J (1995) Plant Canopy Gap-Size Analysis Theory for Improving Optical Measurements of Leaf-Area Index. Applied Optics 34: 6211-6222

Coops NC, Hilker T, Wulder MA, St-Onge B, Newnham G, Siggins A, Trofymow JA (2007) Estimating Canopy Structure of Douglas-Fir Forest Stands From Discrete-Return Lidar. Trees-Structure and Function 21: 295-310

Cote JF, Widlowski JL, Fournier RA, Verstraete MM (2009) The structural and radiative consistency of three-dimensional tree reconstructions from terrestrial lidar. Remote Sensing of Environment 113: 1067-1081

Dubayah R, Bergen K, Hall FG, Hurtt G, Houghton R, Kellndorfer J, Lefsky M, Moorcroft P, Nelson R, Saatchi S, Shugart H, Simard M, Ranson J, Blair JB (2008) Global Vegetation Structure from NASA's DESDynI Mission: An Overview. AGU, San Francisco

Frazer GW, Fournier RA, Trofymow JA, Hall RJ (2001) A comparison of digital and film fisheye photography for analysis of forest canopy structure and gap light transmission. Agricultural and Forest Meteorology 109: 249-263

Hilker T, Coops NC, Culvenor DS, Newnham G, Jupp DLB, Siggins A, Bater CW (2009) Generation of Digital Elevation Models using terrestrial LiDAR. Photogrammetric Engineering and Remote Sensing, submitted

Hopkinson C, Chasmer L (2009) Testing LiDAR models of fractional cover across multiple forest ecozones. Remote Sensing of Environment 113: 275-288

Jonckheere I, Fleck S, Nackaerts K, Muys B, Coppin P, Weiss M, Baret F (2004) Review of methods for in situ leaf area index determination: Part I. Theories, sensors and hemispherical photography. Agricultural and Forest Meteorology 121: 19-35

Jupp DLB, Culvenor DS, Lovell JL, Newnham GJ, Strahler AH, Woodcock CE (2008) Estimating forest LAI profiles and structural parameters using a ground-based laser called 'Echidna'. Tree Physiology 29: 171-181

Jupp DLB, Lovell JL (2007) Airborne and ground-based lidar systems for forest measurement: background and principles. CSIRO Marine and Atmospheric Research Paper 017. CSIRO Marine and Atmospheric Research

Kraus K, Pfeifer N (1999) Determination of terrain models in wooded areas with airborne scanner data. ISPRS Journal of Photogrammetry & Remote Sensing 54: 193-203

Lefsky M, Turner D, Guzy M, Cohen W (2005a) Combining lidar estimates of aboveground biomass and Landsat estimates of stand age for spatially extensive validation of modeled forest productivity. Remote Sensing of Environment 95: 549-558

Lefsky MA, Cohen WB, Acker SA, Parker GG, Spies TA, Harding D (1999) Lidar Remote Sensing of the Canopy Structure and Biophysical Properties of Douglas-Fir Western Hemlock Forests. Remote Sensing of Environment 70: 339-361

Lefsky MA, Cohen WB, Harding DJ, Parker GG, Acker SA, Gower ST (2002a) Lidar Remote Sensing of Above-Ground Biomass in Three Biomes. Global Ecology and Biogeography 11: 393-399

Lefsky MA, Cohen WB, Parker GG, Harding DJ (2002b) Lidar remote sensing for ecosystem studies. BioScience 52: 19-30

Lefsky MA, Harding DJ, Keller M, Cohen WB, Carabajal CC, Espirito-Santo FD, Hunter MO, de Oliveira R (2005b) Estimates of forest canopy height and aboveground biomass using ICESat. Geophysical Research Letters 32

Lim K, Treitz P, Wulder M, St-Onge B, Flood M (2003) Lidar remote sensing of forest structure. Progress in Physical Geography 27: 88-106

Lovell JL, Jupp DLB, Culvenor DS, Coops NC (2003) Using Airborner and Ground-Based Ranging Lidar to Measure Canopy Structure in Australian Forests. Canadian Journal of Remote Sensing 29: 607-622

Magnussen S, Wulder M, Seemann D (2002) Stand canopy estimated by line sampling with airborne lidar. In: K. von Gadow JNaJS (ed) Continuous cover forestry – assessment, analysis, scenarios. Kluwer Academic, Dordrecht/Boston/London, pp 1-12

Miller, JB (1964) An integral equation from phytology. J. Aust. Mathematical Soc. 4:397–402.

Miller, JB (1967) A formula for average foliage density. Aust. J. Bot. 15:141–144

Morgenstern K, Black TA, Humphreys ER, Griffis TJ, Drewitt GB, Cai TB, Nesic Z, Spittlehouse DL, Livingstone NJ (2004) Sensitivity and Uncertainty of the Carbon Balance of a Pacific Northwest Douglas-Fir Forest During an El Nino La Nina Cycle. Agricultural and Forest Meteorology 123: 201-219

Næsset E (1997) Determination of Mean Tree Height of Forest Stands Using Airborne Laser Scanner Data. Isprs Journal of Photogrammetry and Remote Sensing 52: 49-56

Næsset E, Bjerknes KO (2001) Estimating Tree Heights and Number of Stems in Young Forest Stands Using Airborne Laser Scanner Data. Remote Sensing of Environment 78: 328-240

Ni-Meister W, Jupp DL, Dubayah R (2001) Modeling Lidar Waveforms in Heterogeneous and Discrete Canopies. Geoscience and Remote Sensing 39: 1943-1957

Pang Y, Lefsky M, Andersen HE, Miller ME, Sherrill K (2008) Validation of the ICEsat vegetation product using crown-area-weighted mean height derived using crown delineation with discrete return lidar data. Canadian Journal of Remote Sensing 34: S471-S484

Parker GG, Harding DJ, Berger ML (2004a) A portable LIDAR system for rapid determination of forest canopy structure. Journal of Applied Ecology 41: 755-767

Parker GG, Harmon ME, Lefsky MA, Chen JQ, Van Pelt R, Weis SB, Thomas SC, Winner WE, Shaw DC, Frankling JF (2004b) Three-Dimensional Structure of an Old-Growth Pseudotsuga-Tsuga Canopy and Its Implications for Radiation Balance, Microclimate, and Gas Exchange. Ecosystems 7: 440-453

Peddle D, Hall F, LeDrew E (1999) Spectral mixture analysis and geometric optical reflectance modeling of boreal forest biophysical structure. Remote Sensing of Environment 67: 288-297

Riano D, Meier E, Allgower B, Chuvieco E, Ustin SL (2003) Modeling Airborne Laser Scanning Data for the Spatial Generation of Critical Forest Parameters in Fire Behavior Modeling. Remote Sensing of Environment 86: 177-186

Richards P (1983) The three dimensional structure of tropical rain forest. Blackwell, Oxford

Ross JK (1981) The radiation regime and architecture of plant stands. Dr. W. Junk Publishers, The Hague

Schaaf CB, Li XW, Strahler AH (1994) Topographic Effects on Bidirectional and Hemispherical Reflectances Calculated With a Geometric-Optical Canopy Model. Ieee Transactions on Geoscience and Remote Sensing 32: 1186-1193

Strahler AH, Jupp DLB, Woodcock CE, Schaaf CB, Yao T, Zhao F, Yang XY, Lovell J, Culvenor D, Newnham G, Ni-Miester W, Boykin-Morris W (2008) Retrieval of forest structural parameters using a ground-based lidar instrument (Echidna (R)). Canadian Aeronautics Space Inst, pp S426-S440

Van der Zande D, Hoet W, Jonckheere L, van Aardt J, Coppin P (2006) Influence of measurement set-up of ground-based LiDAR for derivation of tree structure. Agricultural and Forest Meteorology 141: 147-160

Warren Wilson J (1965) Stand structure and light penetration, I. Analysis by point quadrats. Applied Ecology 2: 383-390

Welles JM, Cohen S (1996) Canopy structure measurement by gap fraction analysis using commercial instrumentation. Journal of Experimental Botany 47: 1335-1342

Whitehead D, Grace J, Godfrey M (1990) Architectural distribution of foliage in individual Pinus radiata D. Don crowns and the effects of clumping on radiation interception. Tree Physiology 7: 135-155

Wulder MA, Bater CW, Coops NC, Hilker T (eds) (2008a) Advances in laser remote sensing of forests: Status and opportunities. Nova Publishers

Wulder MA, Bater CW, Coops NC, Hilker T, White JC (2008b) The role of LiDAR in sustainable forest management. Forestry Chronicle 84: 807-826